Intermolecular interaction in [C6H10N3]2[CoCl4] complex: Synthesis, XRD/HSA relation, spectral and catecholase catalytic analysis

Abderrahim Titi, Ismail Warad, Monique Tillard, Rachid Touzani, Mouslim Messali, Mohamed El Kodadi, Driss Eddike, Abdelkader Zarrouk

Intermolecular Interactions in $[C_6H_{10}N_3]_2[CoCl_4]$ complex; Synthesis, XRD/HSA relation, spectral and Catecholase catalytic analysis

Abderrahim Titi[a,*], Ismail Warad[b,*], Monique Tillard[c], Rachid Touzani[a], Mouslim Messali[d] Mohamed El Kodadi[a,e], Driss Eddike[f] , Abdelkader Zarrouk[g]

[a] *Laboratory of Applied and Environmental Chemistry, Mohammed first University, Oujda, Morocco (LCAE).*

[b] *Department of Chemistry and Earth Sciences, PO Box 2713, Qatar University, Doha, Qatar*

[c] *ICGM, Université de Montpellier, CNRS, ENSCM, Montpellier, France*

[d]*Department of Chemistry, Taibah University, 30002 Al-Madina Al-Mounawara, SaudiArabia.*

[e] *CRMEF Oriental, Centre Régional des Métiers de l'Education et de Formation Oujda, Morocco*

[f] *Laboratory of Inorganic Solid State Chemistry, Mohammed first University, Oujda, Morocco.*

[g] *Laboratory of Materials, Nanotechnology and Environment, Faculty of Sciences, Mohammed V University, Av. Ibn Battouta, Box 1014, Agdal-Rabat, Morocoo*

Abstract

Complex of bis(6-amino-2,4-dimethylpyrimidin-1-ium) tetrachloridecobaltate(II) $[C_6H_{10}N_3]_2[CoCl_4]$ was synthesized and characterized using several physicochemical surveys as FT-IR, 1H & 13C-NMR, Hirshfeld surface (HSA) and XRD-diffraction analysis. The XRD and HSA quantified a significant contribution of non-covalent H-bonds interactions in lattice to build an ionic form of the $[C_6H_{10}N_3]_2[CoCl_4]$ complex. The molecular arrangement is qualified for the desired complex as an alternation of inorganic and organic species, the organic $C_6H_{10}N_3$ cationic ligand and inorganic $[CoCl_4]^{2-}$ tetrahedral anionic metal center connected together via several short interactions like -HN-H…Cl, Nring-H+…Cl and Cring-H…Cl H-bonds interactions. The complex was tested as a catalyst for the oxidation reaction in methanol from 3,5-ditertiarybutylcatechol to 3,5 ditertiarybutylquinone. The $[C_6H_{10}N_3]_2[CoCl_4]$ complex displays a good catalytic activity in aerobic condition, with a reaction rate Vmax = 10.11×10-4 $M.L^{-1}.h^{-1}$ and key kinetics parameters KM = 0.12 M and kcat = 84.08 $M^{-1}.h^{-1}$.

Keywords: Cobalt(II); Crystal structure; HSA; Catecholase activity.

1. Introduction

Organic and inorganic hybrids material are highly wanted compounds due to their broad range of applicable properties, their exceptional structural and amazing composition diversity [1]. Therefore, the structures of the inorganic anion and organic cations reflected several unique properties like optical, electrical, electroluminescence and magnetic [1-6]. Currently, hybrid organic-inorganic crystalline solids containing anionic metal complexes and organic cations have been developed for their hydrogen bonding like N-H….X connections with halides of the metal center to build and design the crystal structure lattice of hybrid material for structural analysis [7-9]. However, studies dilling with such kind of material is still limited.

Cobalt-organic hybrid material complexes are one of the most significant materials in inorganic chemistry, its advantages include good tunable bandgap, electric mobility, thermal stability, magnetic properties, and structural varieties served it to be very good catalysts [1-6]. Even after the discovery of the famous hydroformylation catalytic process by Otto Roelen, many other catalytic applications have been promoted [10-15]. Design of cobalt-organic hybrid material that can activate molecular oxygen stile a challenge to predict super-oxidation catalysts (SOC) [16]. Synthetic model studies on the reactivity of cobalt complexes towards Catecholase oxidation processes, both implicate structural and electronic parts as being accountable for the catalytic activity [16-18].

Considering the attributes and attractive the of tetrachlorocobaltate(II), herein, we report on the preparation of a new $[C_6H_{10}N_3]_2[CoCl_4]$ complex based on cobalt(II) and (6-amino-2,4-dimethylpyrimidin-1-ium) ligand, the intermolecular interactions in the structure was compared by XRD and HAS, physicochemical and oxidation properties of the complex were also figure out under RT conditions.

2. Experimental

2.1 Materials and physical measurements

All the chemicals reagents and solvents were commercial available and used as received. IR were recorded at RT using a Perkin Elmer FT- IR spectrometer in the 4000-500 cm^{-1} frequency range. ^{1}H and ^{13}C NMR were recorded on a BRUKER equipment at 400 MHz for ^{1}H and 100 MHz for ^{13}C. Spin resonances are presented as chemical shifts (δ) in ppm and referenced as follow to the residual peak of the solvent employed as an internal standard: DMSO-d_6 2.50 ppm (^{1}H NMR), 39.9 ppm (^{13}C NMR). The UV – Vis spectra were recorded on

an UV-1280 Shimadzu spectrometer. The Hirschfeld surfaces have been computed using the Crystal Explorer 3.1 program [19].

2.2 Synthesis of [$C_{12}H_{20}N_6CoCl_4$]

A volume of 10 mL of 2,6-dimethylpyrimidin-4-amine (50 mg, 0.41 mmol) in solution in ethanol) was treated with 10 mL of solution of $CoCl_2.6H_2O$ (96.5 mg, 0.41 mmol) dissolved in ethanol, (35.6 mg, 0.82 mmol) of HCl was added to the reaction mixture (Scheme 1). Precipitation of a blue powder occurred while stirring at room temperature for 24h. The blue powder was filtered and washed with EtOH (30mL), followed by Et_2O (30mL) to give the blue solid (1.3g, 70%). Recrystallization of the crude product from a solvent pair $(CH_3)_2CO/Et_2O$ gave blue crystals (1.2g,64.6%). ^{1}H NMR (DMSO-d6, 400MHz): δ = 2.13 (s, CH_3), 2.25 (s, CH_3), 6.06 (s, C-H), 6.63 (s, NH_2). ^{13}C NMR (DMSO-d6, 100 MHz): δ = 23.71 (CH_3), 25.72 (CH_3), 100.53 (C-H), 164.29 (C), 164.38 (C), 166.99 (C). Selected IR peaks of the desired complex ν = 3350 (N-H), 2934 (C-H), 1678 (C=N), 1490 (C=C), 1436 (C-H), 1358 (N=N), 1018(C-N), 720(C-H), 520 (Co-Cl) cm^{-1}.

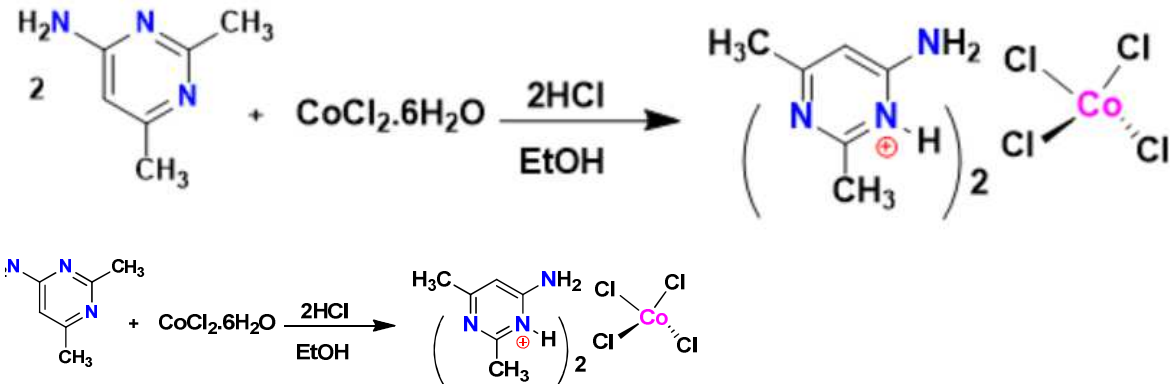

Scheme1: Synthesis of the complex $CoCl_4LH$.

2.3. X-ray crystal structure

A blue platelet was selected under a stereo microscope with a polarizing filter to be a single crystal suitable for diffracted intensities recording. Data were measured at room temperature on a Bruker D8 Venture 4-circle diffractometer equipped with a Incoatec IμS 3.0 Mo microsource (110μm beam, Kα radiation λ = 0.71073 Å) and a Photon II CPAD detector. Cell refinement, data reduction and Lorentz-polarization corrections were performed using the Apex

software suite [20] and reflections were corrected for absorption effects (multi-scan SADABS). The structure was solved and refined by full-matrix least-squares on F^2 using the SHELX programs [21, 22]. Positional and anisotropic displacement parameters were refined for all non-H atoms. The H atoms were detected in the final Fourier difference and, with the exception of the freely refined amine and ammonium H atoms, were treated using AFIX instructions with displacement parameters equal to 1.2 times (1.5 for $-CH_3$) the U_{eq} of the parent atom. The main crystal data and refinement parameters are given in Table 1.

Table 1. Crystal data and refinement parameters of $C_{12}H_{20}N_6CoCl_4$

Chemical formula	$C_{12}H_{20}N_6CoCl_4$
CCDC	1987738
M_r	449.07
Crystal system, space group	Orthorhombic, Pnma
Absorption coefficient (mm^{-1})	1.421
Theta range (°)	2.648 to 29.152
Lattice parameters (Å)	a = 15.3821(4), b = 17.9849(4), c = 7.11250(10)
Crystal size (mm)	0.18 × 0.14 × 0.03
V ($Å^3$),	1967.64 (7), 4
Reflections collected / independent	26837 / 2736 [R(int) = 0.0443]
Data / parameters	2736 / 120
Goodness-of-fit on F^2	1.068
Final R indices [I>2σ(I)]	R1 = 0.036, wR2 = 0.0881
R indices (all data)	R1 = 0.052, wR2 = 0.0993
Extinction coefficient	0.0020(5)
Largest diff. peak and hole ($e.Å^{-3}$)	0.621 / -0.667

3. Results and discussion

3.1. Synthesis, CHN-EA, IR, UV-vis. and NMR analysis

The prepared of bis(6-amino-2,4-dimethylpyrimidin-1-ium) tetrachloridecobaltate(IV) $[C_6H_{10}N_3]_2[CoCl_4]$ Complex was made available by mixing of [1:1] $CoCl_2.4H_2O$ with of 6-amino-2,4-dimethylpyrimidin-1-ium in the presence of HCl dissolved in ethanol. The blue color precipitate indicated the formation of the desired complex with good yield after one day

of stirring under open RT condition. The complex is water-soluble, poor insolubility in ROH and insoluble in hexane or ethers which supported the complex $[C_6H_{10}N_3]_2[CoCl_4]$ salty nature.

The composition of the complex was confirmed using CHN-elemental analysis, the calculated atomic percentage of the C, 32.09; H, 4.49 and N, 13.12% from C12H20Cl4CoN6 formula and found experimentally as C, 32.02; H, 4.20 and N, 13.16% which is with agree with the general $[C_6H_{10}N_3]_2[CoCl_4]$ formula.

The reaction of $CoCl_2.4H_2O$ with 6-amino-2,4-dimethylpyrimidin-1-ium ligand to produce $[C_6H_{10}N_3]_2[CoCl_4]$ complex was monitored by IR. IR spectra of the ligand and its complex are illustrated in Fig. 1.

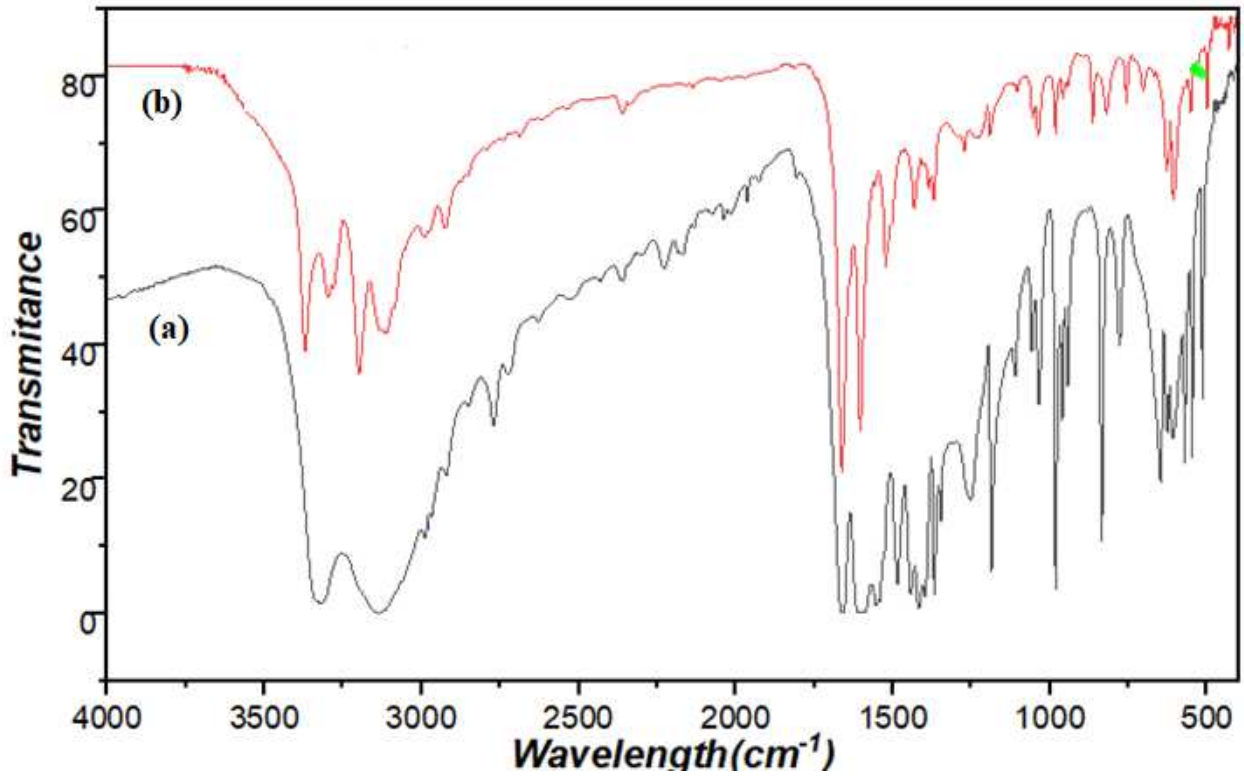

Fig. 1. FT-IR spectra of free ligand (a) and the $[C_6H_{10}N_3]_2[CoCl_4]$ complex (b).

Several stretching vibrations, like N-H, C_{ph}-H, C_{Me}-H, C=N, C-C, C=C and Co-Cl [23] were recorded to their expected chemical shifts (experimental section). The sharp and broad band at 3350 cm^{-1} for N-H in the free ligand did not shift to lower chemical shift by the complexation with the Co center which indicating no Co-N bond formation. Moreover, no new

broad signal ~ 500 cm^{-1} was appearance in the spectrum of the complex supporting the $[C_6H_{10}N_3]_2[CoCl_4]$ salty nature of the desired complex [23-28].

The UV-visible electron transfer spectra of the 1x10-4 M of the desired $[C_6H_{10}N_3]_2[CoCl_4]$ complex in DMSO at RT is illustrated in Fig. 2. The UV band with ƛmax at 280 nm is sited to the π to π* e-transition in the aromatic group of the ligand. Moreover, maximum absorption bands at ƛ's 350-420 nm in the visible area are attributed to d-d e-transition indicating the $[CoCl_4]^{-2}$ with Td geometry around cobalt atom [23-28].

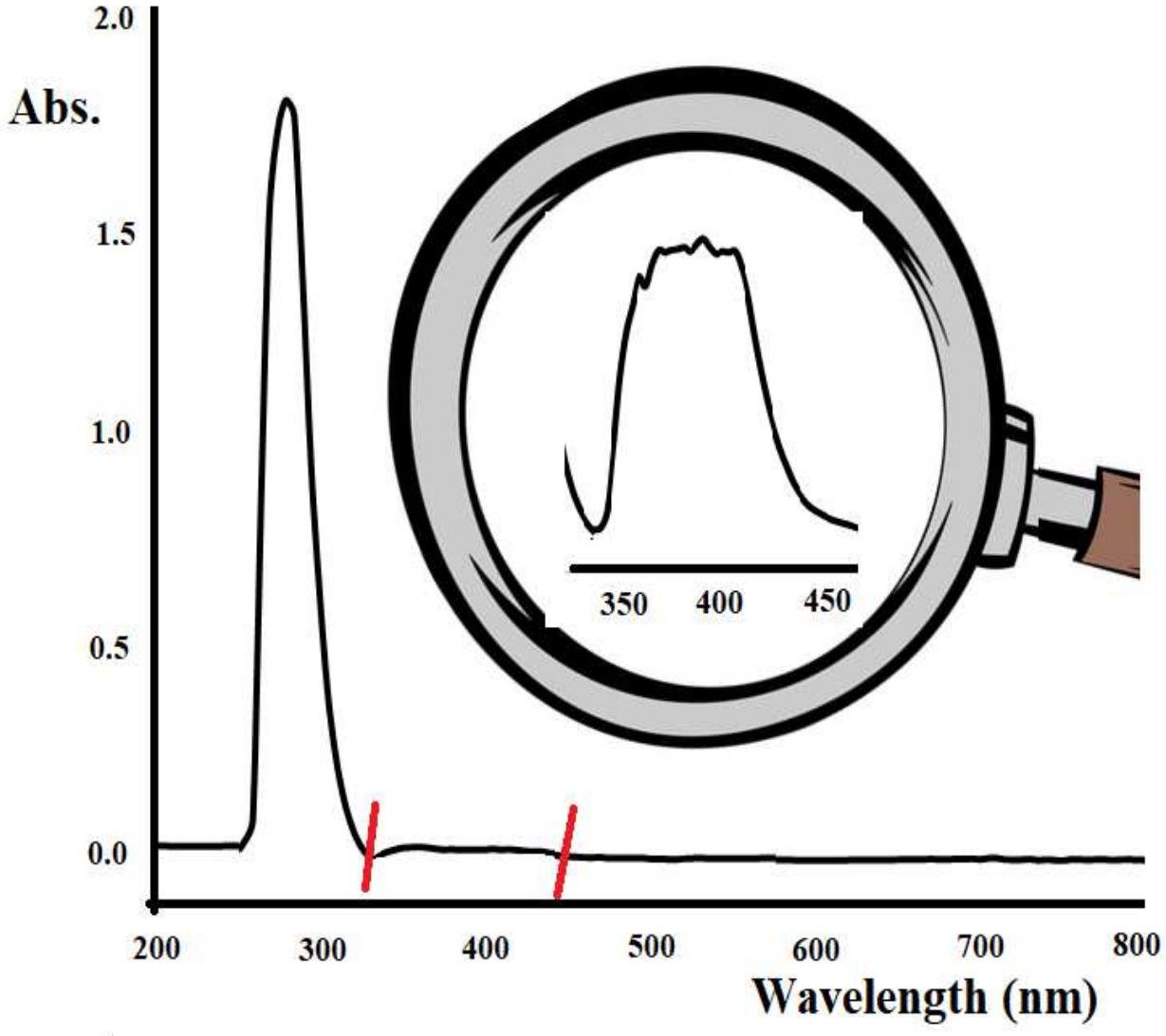

Fig. 2. UV- Visible of $[C_6H_{10}N_3]_2[CoCl_4]$ complex

The ^{1}H and ^{13}C-NMR spectra of $[C_6H_{10}N_3]_2[CoCl_4]$ complex dissolved in DMSO-d6 reflected the complex as paramagnetic compound since the Co is with +2, therefore the electronic configuration of the tetrahedral Co center will be $4s^0 3d^7$ with eg^4 and $t1g^3$ d-splitting.

Two types of protons consistent with the structure formula detected by XRD were recorded as in Fig.3. 1H NMR two signal belong to 6H of the CH3 at δ 2.13 and 2.25 ppm, one signal at 6.06 ppm cited to Cring-H and the broad signal at δ 8.3 cited to 2H of NH2 (Fig.3a). The N-H+ protons signals did not appear due to D-exchanged with the D2O.

13C-NMR spectrum reflected δ's 23.71 and 25.72 belong to 2C of CH3 groups and three signals with δ's 164.29, 164.38, 166.99 ppm belong to the 3C of the aromatic ring (Fig.3b).

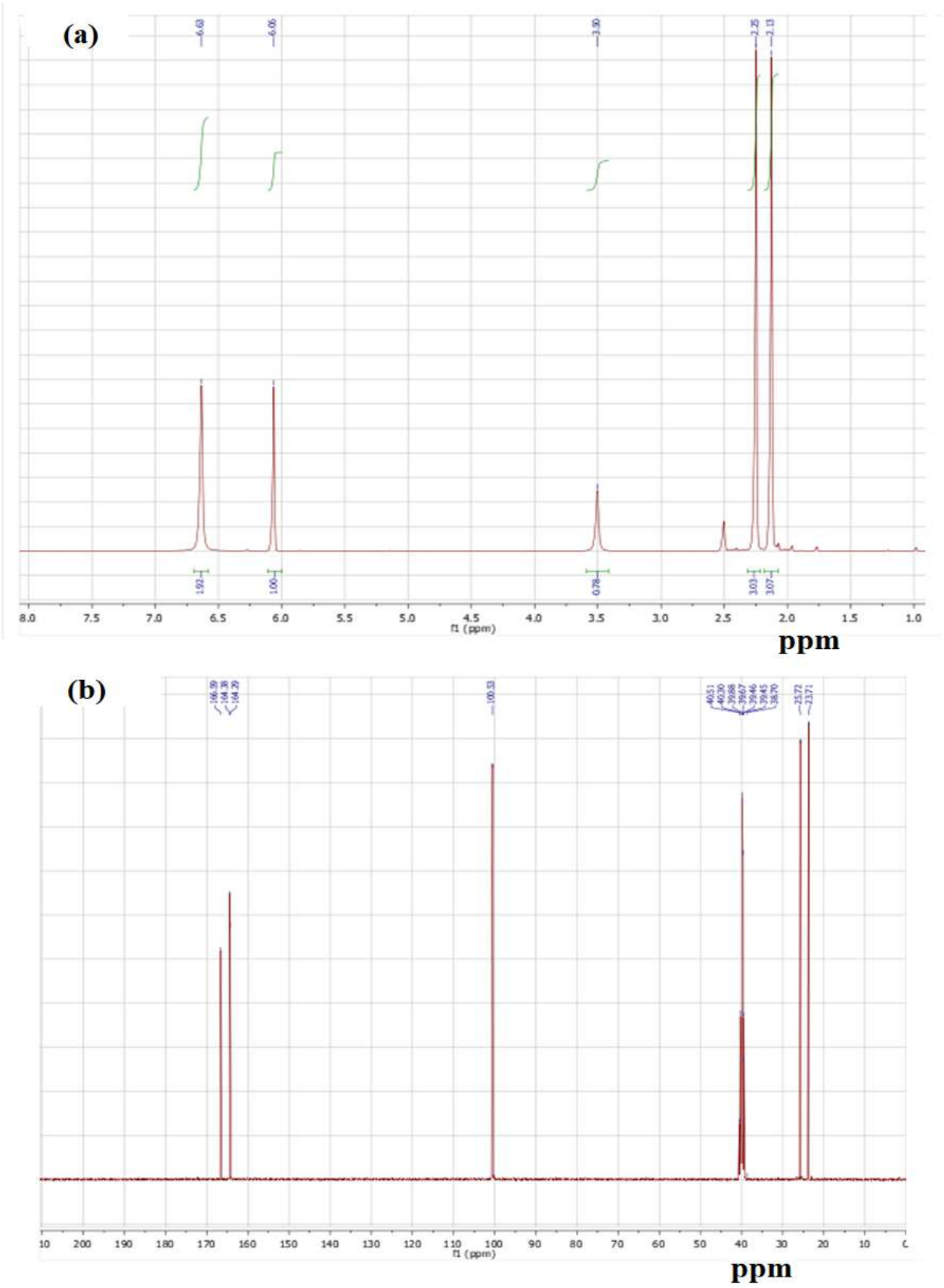

Fig. 3. (a) ^{1}H NMR and (b) ^{13}C NMR spectra in DMSO-d_6

3.2. XRD structural asnd packing analysis

The structure of $[C_6H_{10}N_3]_2[CoCl_4]$ complex is clarified in Fig.4a. Selected bond lengths and angles are listed in Table 2. The reflections were indexed in an orthorhombic lattice of dimensions a = 15.38, b = 17.98, c = 7.11 Å. The unit cell contains four tetrahedral units [CoCl4]2- and eight planar units 6-amino-2,4-dimethylpyrimidin-1-ium (r.m.s. of the fitted atoms to the least square plane is only 0.0194), that is to say, four $(C_6H_{10}N_3)_2CoCl_4$ formula units (Fig. 3). The final refinement converged to R1-factor of 3.58%. Moreover, a regular tetrahedral geometry around the Co(II) center bound by 4 equivalent chlorine antions, with 2.25-2.29 Å Co–Cl average bond lengths and 105.23-113.76° Cl–Co–Cl average angles with slightly deviated from 109.5° as ideal value [23-29].

The extinction conditions suggested centrosymmetry and space group Pnma. The structure contains anionic (-2) tetrachlorocobalt and 2 cationic (+1) 6-amino-2,4-dimethylpyrimidin-1-ium units represented with ORTEP (Fig. 4a).

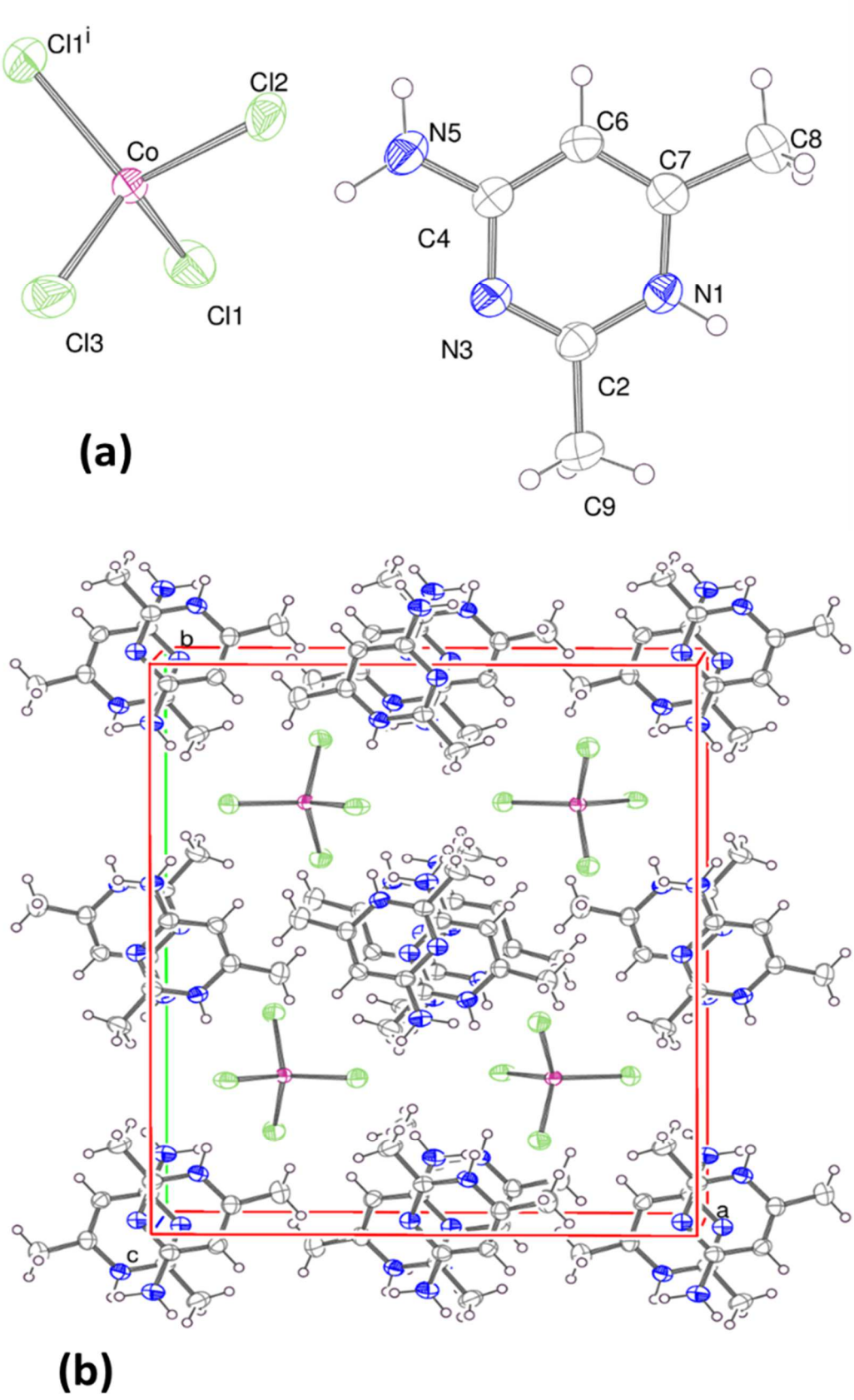

Fig. 4. ORTEP of $[C_6H_{10}N_3]_2[CoCl_4]$ with two molecular units $CoCl_4^{2-}$ & $C_6H_{10}N_3^+$ and (b) the orthorhombic molecular packing lattice of $C_{12}H_{20}N_6CoCl_4$

Table 2. Main bond lengths [Å] in $C_{12}H_{20}N_6CoCl_4$

No.	Bond type		Å	No.	Angle type			(º)
1	Cl1	Co	2.2544	1	Cl1	Co	Cl2	107.32
2	Cl2	Co	2.309	2	Cl1	Co	Cl3	109.58
3	Cl3	Co	2.283	3	Cl1	Co	Cl1	113.01
4	Co	Cl1	2.2544	4	Cl2	Co	Cl3	109.98
5	N1	C2	1.346(3)	5	Cl2	Co	Cl1	107.32
6	N1	C7	1.361(3)	6	Cl3	Co	Cl1	109.58
7	C2	N3	1.313(3)	7	C2	N1	C7	122.2(2)
8	C2	C9	1.488(4)	8	N1	C2	N3	122.2(2)
9	N5	H5A	0.98(5)	9	N1	C2	C9	117.6(2)
10	N5	C4	1.333(3)	10	N3	C2	C9	120.2(2)
11	N5	H5B	0.89(3)	11	H5A	N5	C4	121(2)
12	N3	C4	1.366(3)	12	H5A	N5	H5B	118(3)
13	C8	C7	1.485(4)	13	C4	N5	H5B	121(2)
14	C4	C6	1.404(3)	14	C2	N3	C4	117.3(2)
15	C7	C6	1.351(3)	15	N5	C4	N3	116.6(2)

In the crystal lattice, four types of non-covalent bonds shorter than 3 Å was detected by XRD measurements, since two polar H atoms together with three types of N atoms quoted in the complex structure, therefore, 4 types of H-bond linkages were recorded experimentally in the packed lattice of the desired complex as two types of –HN-H…..Cl with 2.307 Å and -–HN-H…..Cl….. H-NH with 2.463 Å as illustrated in Fig.5a. one longer H-bonds were detected as –Nring-H…..Cl….. H-Nring with 2.385 Å (Fig.5b). Furthermore, 2 longer H-bonds were recorded as –Cring-H…..Cl with 2.888 Å (Fig.5c), no other interaction types were recorded.

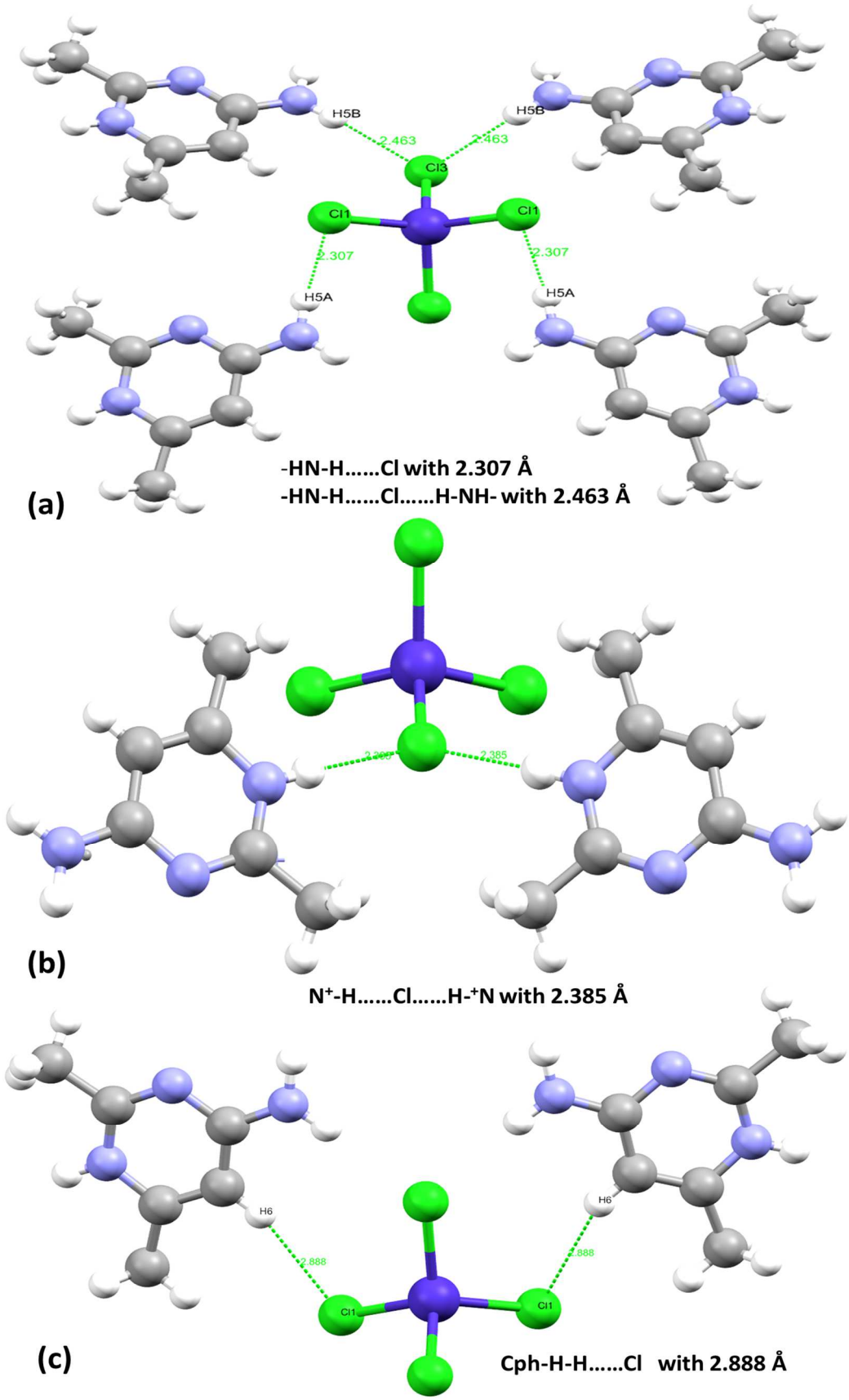

Fig. 5. H-bonds interaction: a) –HN-H…..Cl & –HN-H…..Cl….. H-NH, b) –N_{ring}-H…..Cl….. H-N_{ring} and (c) –C_{ring}-H…..Cl.

3.3. HSA

To obtain additional information on the role played by intermolecular interactions within the crystal, a Hirshfeld surface analysis was performed [29-32]. The results are illustrated in Fig. 3 with representations of the Hirshfeld three dimensional surface mapped over the normalized d_{norm} function (Fig.6) and shape index (Fig. 6b) established in the range 0.654 to 1.768 a. u.

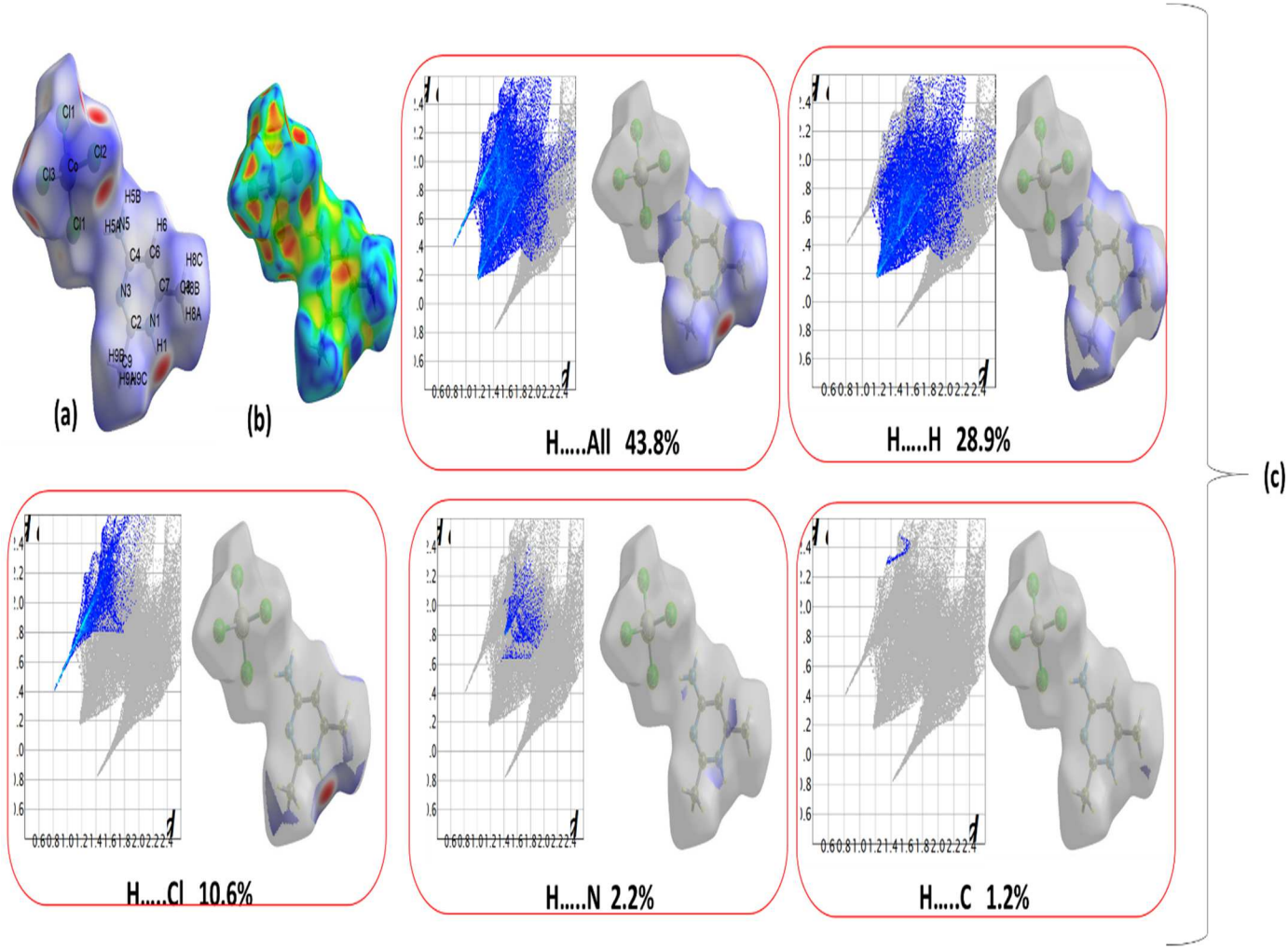

Fig.6. Hirshfeld surface mapped over d_{norm} (a), shape index (b) and inside/outside 2-D fingerprint plots (c).

The colors are related to the distance from the nearest neighbors and illustrate the strength of the intermolecular contacts. Large red zones are visible close to the chlorine atoms and the polar hydrogen atoms, six red spots were found on the surface computed for the molecular structure, they correspond to the presence of three short contacts or hydrogen type bonds. Two N-H…..Cl bonds with a distance of 2.38 Å, two NH_2…..Cl bonds with a distance of 2.31 Å and two Cring-H….Cl with a distance of 3.17 Å was counted in good agreement with packing in the crystal structure.

The 2D fingerprint plots represented in Fig. 6b has been built from the 3D Hirshfeld surface by considering inside and outside closest neighbors. These integrated views on intermolecular contacts are useful to visualize the contributions of either polar or non-polar interactions to the crystal packing forces. It is clear that the H…H intermolecular contacts represent the larger part (28.9%), which is due to the high number of H-atoms and their spatial position in the molecule of the complex. In contrast, the H….N interactions are found with the lowest and almost zero ratios. The other atom…atom intermolecular contacts appear in the order of importance H….Cl (10.6%) > H….N (2.2%) > H….C(1.2%).

3.4 Catecholase studies

3.4.1. catecholase activity via UV-Vis study

The catecholase activity of the complex was observed by treating 10^{-4} M solution of complex with 100 equivalents of 3,5-DtBC (10^{-2} M) solution under aerobic fitness at room temperature in MeOH, as seen in Scheme 2.

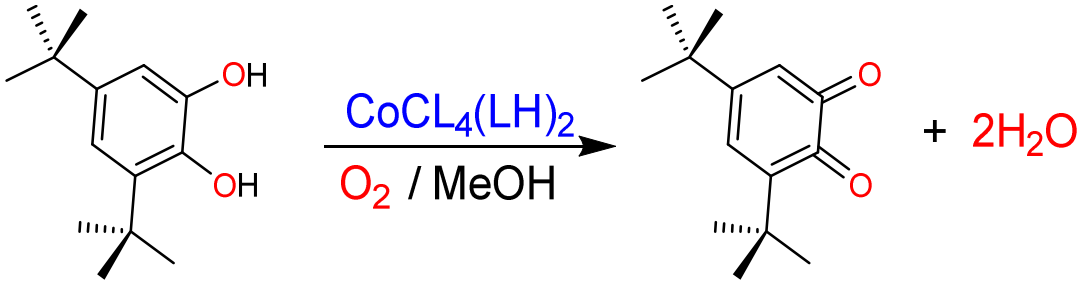

Scheme 2. Catalytic oxidation of 3.5-DtBC to 3,5-DtBQ.

The above oxidation process was monitored by UV-vis., the Spectrophotometric data have been noted by generating absorbance versus wavelength (λ= 400 nm scan) plots at a regular time intervals of 5 min in the range 325−625 nm (Fig.7a). The 3,5-DtBQ product band appeared at 400 nm which graduately increases in intensity by time reflected the completeness of the reaction, No absorbance at this band was observed in the absent of $[C_6H_{10}N_3]_2[CoCl_4]$ or even in the presence of $CoCl_2.6H_2O$ using the 3,5-DtBC substrate (Fig.7b) , therefore, it is clearly observed that $[C_6H_{10}N_3]_2[CoCl_4]$ acted as a mild condition catalyst in absence of complex as indicated by the black curve. It clearly appears that the complex drives the oxidation reaction of 3,5-DtBC to 3,5-DtBQ under mild conditions.

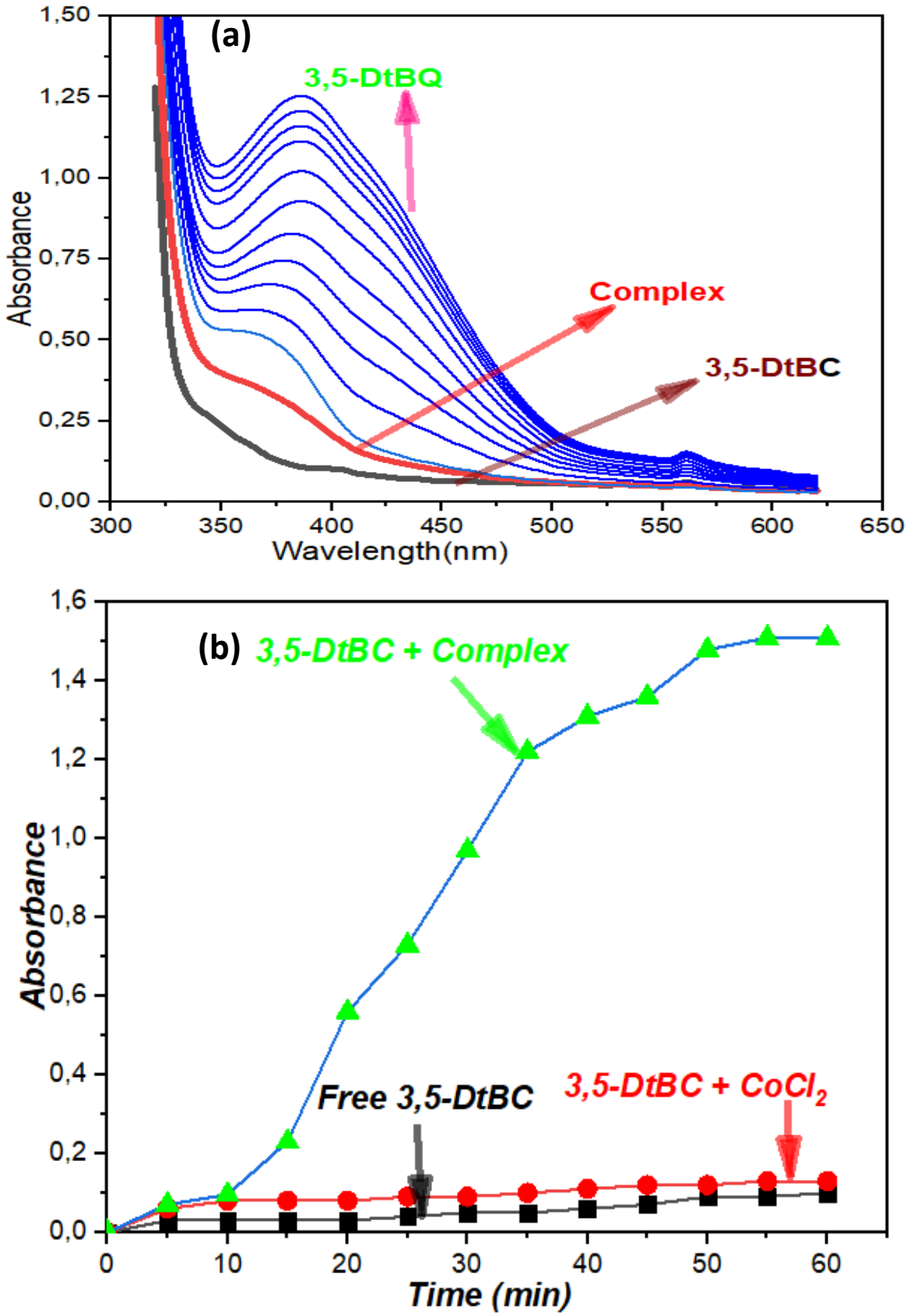

Fig. 7. (a) Wavelength scan and (b) Abs. *vs.* time (at λ = 400 nm) plots for the oxidation of 3,5-DtBC to 3,5-DtBQ in the absence and presence of the $[C_6H_{10}N_3]_2[CoCl_4]$ complex.

4.2. Kinetic study

A kinetic approach based on the Michaelis-Menten procedure was applied and the results were deduced from the non-linear Michaelis-Menten hyperbolic plots. Control experiments were conducted for the Cobalt (II) chloride salt and for the ligand (L) to identify any singular influences on the oxidation of 3,5-DtBC [33-36]. The concentration of the complex was (10-3 mol.L-1) and the 3,5-DtBC concentration was varied in the range 5, 10, 20, 40, 60 and 80 equivalents. The progression of absorbance of 3,5-DtBQ at 400 nm was controlled for the first 5 minutes of the reaction time, and the linear correlation for the prime rates and the substrate concentration was collected. The rate versus concentration data for the substrate was examined on the basis of Michaelis–Menten approach of enzymatic kinetics to get the Lineweaver–Burk (double reciprocal) plot as well as the values of the various kinetic parameters. The kinetic study for the complex shows that applying the Michaelis-Menten model to determine kinetic parameters leads to Vmax speed of 16.82 µM.L-1.min-1 and kinetic parameters Km of 0.12 M and kcat of 84.08 M-1.h-1. As clearly shown on the graphic representation of rates (V) as a function of the substrate concentration progression (Fig. 8), the reaction rate increases immediately and reaches its maximum for about 10 equivalents of 3,5-DtBC .

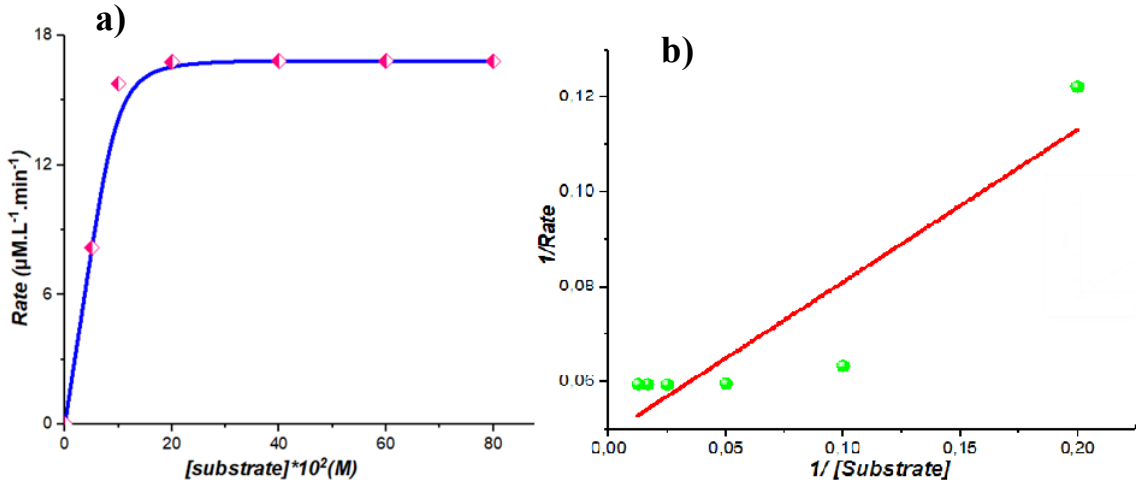

Fig. 8. ***a)*** Enzymatic Michaelis-Menten Kinitic plot (rate *vs.* [substrate]) and **b)** Lineweaver-Burk plot (1/rate *vs.*1/[substrate] for the complex in MeOH.

Table 4. A comparison of V_{max}, K_M and k_{cat} values reported in the litterature for cobalt complexes in the oxidation of 3,5-DtBC to 3,5-DtBQ

Complex & ref.	V_{max} ($M.L^{-1}.min^{-1}$)	K_M (M)	k_{cat} (h^{-1})	k_{cat} / K_M $M^{-1}.h^{-1}$	Solvent

$CoCl_4(LH)_2$	16.82×10^{-6}	12.103×10^{-2}	10.09	84.08	MeOH
[26]	18.91×10^{-6}	15.7×10^{-4}	45.38	28.9×10^{3}	MeOH
[27]	3.40×10^{-4}	1.89×10^{-4}	11.2	59.25×10^{3}	DMF
[28]	1.5×10^{-6}	24.7×10^{-4}	0.9	364	MeOH
[28]	11.7×10^{-6}	27.7×10^{-4}	7.02	2534	MeOH
[26]	7.14×10^{-6}	24.5×10^{-4}	42.9	17510	THF
[28]	1.9×10^{-6}	24.7×10^{-4}	1.14	461	CH_3CN

To properly establish the catalytic activity of the 3,5-DtBC on the production kinetics of 3,5-DtBQ, a volume of 0.15 mL of complex (1×10^{-4}M) dissolved in methanol was added to 2 ml of 3,5-DtBC (1×10^{-1} M), and then the spectral variations were quantified using the progression of the absorbance band characteristic of the 3,5-DtB-quinone registered every 5 min. The kinetic experiments were realized at room temperature.

4. Conclusion

During this work, we synthesized a $[C_6H_{10}N_3]_2[CoCl_4]$ complex designed by 6-amino-2,4-dimethylpyrimidin-1-ium ligand and $CoCl_2.6H_2O$ salt. The complex is described by various spectroscopic techniques as ^1H & ^{13}C NMR, UV-vis., FT-IR, CHN-EA and HSA. The structure of [$\mathbf{C_{12}H_{20}N_6CoCl_4}$] was proved by XRD-diffraction. The XRD reflected the tetrachloridecobaltate(II) anion as tetrahedral geometry around the cobalt center. The HSA and XRD analysis supported the presence of many H-bond like of –HN-H…..Cl with 2.307 Å and -–HN-H…..Cl….. H-NH with 2.463 Å,–N_{ring}-H…..Cl….. H-N_{ring} with 2.385 Å and –C_{ring}-H…..Cl with 2.888 Å distances.

The complex displays a good catalytic behavior, under ambient conditions, estimate to the oxidation of 3,5-D*t*BC to 3,5-D*t*BQ using atmospheric oxygen as oxidant in methanol. Overall the catalytic activity of the $[C_6H_{10}N_3]_2[CoCl_4]$ complex is found very similar to that of some other cobalt complexes.

References

[1] C. R. Kagan, D. B. Mitzi, C. D. Dimitrakopoulos, Transistors, Sci. 286 (1999) 945.

[2] J. L. Knutson, J. D. Martin, D. B. Mitzi, Inorg. Chem. 44 (2005) 4699.

[3] T. Sekine, T. Okuno, K. Awaga, Mol. Cryst. Liq. Cryst. 279 (1996) 65.

[4] C. Aruta, F. Licci, A. Zappettini, F. Bolzoni, F. Rastelli, P. Ferro, T. Besagni, Appl. Phys. A 81 (2005) 963.

[5] J-C. Chang, W-Y Ho, I-W Sun, Y-K Chou, H-H Hsieh, T-Y Wu, , Polyhedron 30 (2011) 497.

[6] K. Chondroudis, D. B. Mitzi, , J. Chem. Mater. 11 (1999) 3028.

[7] C.J. Adams, A.L. Gillon, M. Lusi, A.G. Orpen, CrystEngComm 12 (2010) 4403.

[8] I. Baccar, F. Issaoui, F. Zouari, M. Hussein, E. Dhahri, M.A. Valente, Solid State Commun. 150 (2010) 2005-2010.

[9] C. Decaroli, A.M. Arevalo- Lopez, C.H. Woodall, E.E. Rodriguez, c J.P. Attfield, S.F. Parkerd, C. Stock, Acta Crystallogr. B71 (2015).

[10] J. Falbe, Carbon Monoxide in Organic Synthesis, vol 10, Springer Science & Business Media, 2013.

[11] F. Hebrard, P. Kalck, Chem. Rev. 109 (9) (2009) 4272.

[12] R.F. Heck, D.S. Breslow, J. Am. Chem. Soc. 83 (19) (1961) 4023.

[13] G.O. Spessard, G.L. Miessler, Organometallic Chemistry, 2009.

[14] C. Brown, G. Wilkinson, Inorg. Phys. Theor. (1970) 2753.

[15] R.K. Hocking, T.W. Hambley, Organometallics 26 (11) (2007) 2815.

[16] M. F. Kamaruzaman, Y. H. Taufiq-Yap, D. Derawi, Biomass and Bioenergy 134 (2020) 105476.

[17] T. Deelen, H.Yoshida, R. Oord, J. Zečević, B.M. Weckhuysen, K.P.de Jong, Appl. Cat. A: General, 593 (2020) 117441.

[18] L. Li, JingXu, Appl. Surf. Sci. 505 (2020) 143937.

[19] S. K. Wolff, D. J. Grimwood, J. J. McKinnon, D. Jayatilaka, and M. A. Spackman (2007). Crystal explorer 2.1. University of Western Australia, Perth.

[20] Bruker, APEX3. Version 2017.3-0, Bruker AXS, Inc., Madison, Wisconsin, USA, 2017

[21] G. M. Sheldrick, Acta Crystallogr., Sect. A: Fundam. Crystallogr., 71 (2015) 3.

[22] G. M. Sheldrick, Acta Crystallogr., Sect. C: Cryst. Struct. Commun., 71 (2015) 3.

[23] M. Maha, D. E. Janzen, R. Mohamed, S. Wajda, J Supercond Nov Magn, 29 (2016) 1573.

[24] F. Issaoui, W. Amamou, M. Bekri, F. Zouari, E. Dhahri, M.A. Valente, J. Mol. Struc. 1189 (2019) 175.

[25] M. Tahenti, S. Gatfaoui, N. Issaoui, T. Roisnel, H. Marouani, J. Mol. Struc., 1207 (2020) 127781.

[26] O. Moussa, H. Chebbi, M. Zid, J. Mol. Struc., 1180 (2020) 72.

[27] A. Tounsi, S. Elleuch, B. Hamdi, R. Zouari, A.Salah, J. Mol. Struc., 1141 (2019) 512.

[28] R. Debabis, W. Amamou, N. Chniba-Boudjada, F. Zouari, J. Phys. Chem. Solids, 124 (2019) 296.
[29] A. Titi, T. Shiga, H. Oshio, R. Touzani, B. Hammouti, M. Mouslim, I. Warad, J. Mol. Struc. 1199 (2020) 126995.
[30] A. Barakat, M.S. Islam, A.M. Al-Majid, H.A. Ghabbour, S. Atef, A. Zarrouk, I. Warad, J. Theor. Comput. Chem. 17 (2018) 1850005.
[31] I. Warad, F. F. Awwadi, B. Abd Al-Ghani, A Sawafta, N. Shivalingegowda, N. K. Lokanath, M.S. Mubarak, T. Ben Hadda, A. Zarrouk, F. Al-Rimawi, A. B. Odeh, S. A. Barghouthi, Ultrasonics Sonochem. 48 (2018) 1.
[32] M. Aouad, M. Messali, N. Rezki, M. A. Said, D. Lentz, L. Zubaydi, I. Warad, J. Mol. Struc. 1180 (2019) 455.
[33] P. Chakraborty, S. Mohanta, Inorg. Chim. Acta 435 (2015) 38.
[34] S. Majumder, S. Mondal, P. Lemoine and S. Mohanta, Dalton Trans., 42 (2013) 4561.
[35] J.-H. Qiu, Z.-R. Liao, X.-G. Meng, L. Zhu, Z.-M. Wang and K.-B. Yu, Polyhedron, 24 (2005) 1617.
[36] A. Banerjee, A. Guha, J. Adhikary, A. Khan, K. Manna, S. Dey, E. Zangrando and D. Das, Polyhedron, 60 (2013) 102.